

# Periodic orbit effects on conductance peak heights in a chaotic quantum dot

L. Kaplan\*

Department of Physics and Institute for Nuclear Theory,  
University of Washington, Seattle, WA 98195

We study the effects of short-time classical dynamics on the distribution of Coulomb blockade peak heights in a chaotic quantum dot. The location of one or both leads relative to the short unstable orbits, as well as relative to the symmetry lines, can have large effects on the moments and on the head and tail of the conductance distribution. We study these effects analytically as a function of the stability exponent of the orbits involved, and also numerically using the stadium billiard as a model. The predicted behavior is robust, depending only on the short-time behavior of the many-body quantum system, and consequently insensitive to moderate-sized perturbations.

## I. INTRODUCTION

Quantum dots, semiconductor devices in which electrons are confined to live inside a two-dimensional mesoscopic-sized region, have generated much experimental and theoretical interest in the past decade [1]. In the Coulomb blockade regime [2], the dot is weakly coupled to the outside through two narrow or tunneling leads, and individual resonances can be observed when the Fermi energy in the leads matches the energy of a state of  $N$  electrons in the dot. As a function of the Fermi energy or gate voltage one then observes a series of peaks in the conductance, the peak width being controlled by the temperature and the spacing between them by the classical charging energy required to add one more electron to the dot (in the experimentally typical regime where the level spacing is large and the intrinsic resonance width small compared with the temperature). The conductance peak height of the  $n$ -th resonance is then given by

$$G_n = \frac{e^2}{h} \frac{\pi}{2kT} g_n, \quad (1)$$

where

$$g_n = \frac{\Gamma_{an}\Gamma_{bn}}{\Gamma_{an} + \Gamma_{bn}}, \quad (2)$$

and  $\Gamma_{an}$ ,  $\Gamma_{bn}$  are the partial decay widths of the  $n$ -th resonance through each of the two leads labeled  $a$  and  $b$ .

Each of the two partial widths is given by Fermi's Golden Rule as the square of a tunneling matrix element. This matrix element in turn is obtained (in the

single-particle picture) by taking the overlap of the normal derivative of the  $n$ -th dot wavefunction along the boundary with the electron wavefunction in the lead [3,4]:

$$\Gamma_{an} = C_a |\langle \partial_{\perp} \Psi_n | \phi_a \rangle|^2 \quad (3)$$

(and similarly for  $\Gamma_{bn}$ ), where  $\phi_a$  is the relevant transverse wavefunction in lead  $a$ ,  $\partial_{\perp} \Psi_n$  is the normal derivative of the  $n$ -th dot eigenstate at the boundary, and  $C_a$  is a constant associated with the height of the barrier (possibly  $C_a \neq C_b$  if the two leads are unequally coupled). Because tunneling will always be dominated by the lead mode which has the largest longitudinal energy, we may without loss of generality restrict ourselves to  $\phi_a$  which is the lowest transverse energy mode of the lead [3]. For a smooth lead potential, this will be given by a Gaussian,

$$\phi_a \sim e^{-(q-q_0)^2/2\sigma^2}, \quad (4)$$

where the width  $\sigma \sim \sqrt{\hbar}$  depends on the detailed properties of the lead.

Of course in reality the multi-electron state inside the dot is not given by a product of single-particle states, nor do we know the electronic Hamiltonian inside the dot well enough to have any realistic hope of being able to compute the wavefunctions  $\Psi_n$ . We will come back to these important issues in the next section.

Many authors [5] have studied the behavior of the conductance peaks  $G_n$  in the context of random matrix theory. There the overlaps  $\langle \partial_{\perp} \Psi_n | \phi_a \rangle$  are considered as random Gaussian variables (real or complex), and thus the widths  $\Gamma_{an}$ ,  $\Gamma_{bn}$  become  $\chi^2$  random variables of one or two degrees of freedom in the absence or presence of a magnetic field, respectively. These predictions have compared favorably with the experimental data [6]. In the present work, we extend these dynamics-free results to include the effects of short-time dynamics on the distribution of conductance peak heights through a ballistic dot. In doing so, we are following the work of Narimanov, Cerruti, Baranger, and Tomsovic [3] who have already treated the special case of two leads placed symmetrically on the horizontal-bounce orbit of a stadium billiard (though focusing on peak-to-peak correlations, rather than on the peak heights themselves, in contrast with the present work). Here we consider in full generality the short-time classical effects on conductance peak heights, including the dependence of the peak distribution on the stability exponents of the short orbit or orbits near which one or both leads may be located. We also disentangle the effects of symmetry lines and symmetric lead placement from the effects of short-time classical dynamics.

---

\*lkaplan@phys.washington.edu

We note that although quantum dot experiments provide one of the motivations for the present work, the effects we are considering are relevant to a wide variety of physical situations where observable properties are affected by the statistical properties of wavefunctions. In particular, the conductance problem discussed here is formally analogous to a situation often encountered in molecular or nuclear physics, where a reaction  $A \rightarrow B \rightarrow C$  takes place through an intermediate or transition state  $B$  living inside a metastable “well,” and the reaction rate is then determined by the structure of the wavefunction  $B$  inside the well.

The paper is organized as follows: in Section II we briefly review some recent results concerning short-time dynamical effects on wavefunction intensities. We focus in particular on the separation of scales between the bounce time in the dot and the time at which eigenstates are resolved, and on the consequent robustness of short-time effects on *statistical* wavefunction properties. In Section III we analyze the effects of short periodic orbits (s.p.o.’s) on conductance peak statistics for several qualitatively different situations: one lead on a s.p.o., two leads on the same s.p.o., and two leads on different s.p.o.’s for which the spectral envelopes may be in or out of phase with each other in the energy range of interest. Numerical tests of these predictions appear in Section IV, followed by concluding remarks in Section V.

## II. SCARS AND WAVEFUNCTION INTENSITIES: BASIC RESULTS

The scar effect is one of the most visually striking aspects of quantum chaotic behavior. It was noticed already in the 1980’s that the quantum wavefunctions of classically chaotic systems display anomalous enhancement and suppression of intensity in the vicinity of the unstable periodic orbits, contrary to the naive expectation of wavefunction randomness and uniformity [7]. The early theories of this phenomenon [8] treated the short-time linearized dynamics around an unstable orbit, and thus made predictions about energy-smoothed spectral properties. More recently, theories of scars were extended to include long-time nonlinear recurrences, making possible predictions about the distribution of individual eigenstate intensities on a given periodic orbit [9]. The scar formalism has also been adapted to study quantitatively wavefunction structure in systems as varied as Sinai-type billiards and in two-body random interaction ensembles in nuclear physics.

The key result of this work that we need for the present analysis is that wavefunction intensities in a closed system are given by

$$|\langle \Psi_n | \phi \rangle|^2 = r_n S_\phi^{\text{smooth}}(E_n), \quad (5)$$

where  $S_\phi^{\text{smooth}}(E)$  is a smooth local density of states appropriate to the test state  $\phi$ , and the  $r_n$  are random  $\chi^2$

variables. The smooth envelope can be determined by Fourier transforming the short time autocorrelation function of  $\phi$ :

$$S_\phi^{\text{smooth}}(E) = \text{FT}[A_\phi^{\text{short}}(t)], \quad (6)$$

where

$$A_\phi^{\text{short}}(t) = \langle \phi | \phi(t) \rangle e^{-t^2/T_0^2} \quad (7)$$

with some cutoff time  $T_0$ . Now as long as the cutoff  $T_0$  is chosen to be small compared with the Ehrenfest time, which scales as the inverse Lyapunov exponent of the system times  $\log(k_F L)$  ( $L$  being the size of the dot), the short-time dynamics of the wavepacket  $\phi$  may be determined semiclassically, using classical motion linearized around the center of the wavepacket.

In particular, let  $\phi$  (which we will later identify with  $\phi_a$ ) be a Gaussian wavepacket centered on an unstable periodic orbit of period  $P$ . Then we have for  $t = mP$  [10]

$$A_\phi^{\text{short}}(t) = \frac{e^{-im\theta}}{\sqrt{\cosh \beta m + iQ \sinh \beta m}}, \quad (8)$$

where  $\beta > 0$  is the instability exponent for one iteration of the periodic orbit,  $-\theta$  is the classical action in units of  $\hbar$  (plus Maslov indices, if any), and  $Q$  is a non-optimality parameter. The largest recurrences ( $Q = 0$ ) are obtained when the initial wavepacket  $\phi$  is optimally oriented with respect to the stable and unstable manifolds of the orbit. For a lead located on a fixed periodic orbit,  $Q$  will in general be a function of the width  $\sigma$  of the Gaussian mode in the lead (see Eq. 4 and Ref. [10]). More important than the analytic form of Eq. 8, however, is the fact that for weakly unstable orbits (strictly  $\beta \ll 1$ , though due to numerical factors  $\beta \approx 2$  is already in a sense “weak”), strong recurrences in  $A(t)$  persist for  $O(\beta^{-1})$  periods. In the energy domain, we get bumps in the smoothed local density of states  $S_\phi^{\text{smooth}}(E)$ , of width  $O(\beta) \ll 1$  compared to the spacing between the bumps, and of height  $O(\beta^{-1}) \gg 1$  compared to the mean. Very roughly speaking then,  $O(\beta)$  of all wavefunctions are “scarred” on the periodic orbit, having intensity there  $O(\beta^{-1})$  greater than the mean, while most of the remaining wavefunctions are “antiscarred,” their intensity on the periodic orbit being much smaller than the mean. This separation of wavefunctions into scarred and antiscarred ones is of course only a oversimplified picture and one can obtain quantitatively the full distribution of wavefunction intensities on the orbit as a function of the exponent  $\beta$ ; such a comparison between an analytic result for the tail of the intensity distribution and numerical data was in fact performed in [11]. One can also study the moments of the intensity distribution, and finds, for example, that the mean squared intensity approaches  $\pi/\beta$  times the RMT expectation for small  $\beta$  (in units where the mean intensity is normalized to one).

We emphasize the distinction between scar predictions and the brute-force semiclassical computation of chaotic

wavefunctions [12]. In many physically interesting situations, the Hamiltonian of the system is not known nearly well enough to compute individual eigenlevels and eigenstates either semiclassically or indeed using the full quantum machinery. What is of interest in such situations is not so much the detailed structure of the  $n$ -th eigenstate in a given sample, but rather attaining a theoretical understanding of the statistical properties of the system. In a billiard (hard wall) system, changing the boundary by even one square wavelength far away from the periodic orbit of interest will already destroy the detailed structure of individual wavefunctions on the orbit, but will not affect statistical properties such as the distribution of intensities on the orbit. In the time domain we see this easily by recognizing that to resolve individual eigenstates requires following the dynamics to times of order of the Heisenberg time, which scales as  $\hbar$  over the mean level spacing, or  $O(k_F L)$  bounce times in  $d = 2$ . Scar predictions, on the other hand, only require short-time dynamical information, on the scale of the one-bounce time  $T_B$  (or, to get the full effect, the classical Lyapunov decay time  $T_B/\beta$  if the instability exponent  $\beta$  is small). Thus, deformations of the Hamiltonian will not affect these statistical predictions as long as the mean free path associated with such deformations is larger than the sample size  $L$  (i.e. as long as we truly remain in the ballistic regime).

In the energy domain, the mean level spacing in  $d = 2$  goes as  $1/L^2$  (in units where  $m, \hbar \sim 1$ ), while the scale associated with scar effects (i.e. the separation between the bumps in the smooth local density of states envelope) is  $1/T_B \sim k_F/L$ . Thus a single bump in the LDOS corresponds to  $O(k_F L) \gg 1$  level spacings, and in the high-energy regime (i.e. many electrons in the dot) the resulting wavefunction intensity statistics will be quite insensitive even to perturbations that are large compared with the mean level spacing.

The preceding argument applies also to electron-electron scattering effects. It is known that a rather weak interaction beyond mean field will completely destroy level repulsion and cause the distribution of level spacings to approach a Gaussian form, in strong contrast with the Wigner-Dyson prediction of the single-particle theory [13]. The Gaussian behavior is indeed what is observed experimentally in such systems. This is not surprising because strong multi-particle effects on the level spacing scale require only that the interaction mean free path be smaller than the very large Heisenberg scale  $\sim (k_F L)T_B$ . On the other hand, as we have seen, the effects on wavefunction statistics will be weak as long as an individual electron can freely travel across the device before interacting.

It is also known (by comparing the ground state of a dot with  $N$  electrons with the excited states of the same dot containing only  $N' < N$  electrons) that adding electrons to the dot changes the shape of the mean field potential and thus has a significant effect on the character of the single-particle states. Arguments very similar

to those in the preceding paragraphs tell us that a very small change in the effective potential (resulting in matrix elements of the perturbation which are of order of the mean level spacing) is sufficient to destroy our predictive power for individual wavefunctions, but does not affect the *statistical* properties of these wavefunctions, which are associated with a much shorter time scale (the bounce time) and are therefore robust to any such perturbation. The statistical predictions would become irrelevant only if adding one or a few electrons to the dot changed the resulting potential in such a way as to completely change the character of the short classical trajectories.

### III. CONDUCTANCE PEAK HEIGHTS IN CHAOTIC SYSTEMS

#### A. Generically placed leads

Within the context of RMT, Alhassid and Lewenkopf [14] have derived an explicit form for the distribution of conductance peak heights  $g_n$ , allowing for the possibility of unequal leads ( $C_a \neq C_b$  above) and also allowing for correlated channels. In the presence of time reversal symmetry,<sup>1</sup> for two leads consisting of one channel each, this distribution reduces to

$$\begin{aligned}
 P(g) &= \int_{1/2s_a}^{\infty} d\tau \int_{1/2s_b}^{\infty} d\tau' \frac{(4g/2\pi^2) e^{-(\tau+\tau')g}}{\sqrt{(s_a\tau - 1/2)(s_b\tau' - 1/2)}} \\
 &\times \left[ K_0(2g\sqrt{\tau\tau'}) + \frac{1}{2} \left( \sqrt{\frac{\tau}{\tau'}} + \sqrt{\frac{\tau'}{\tau}} \right) K_1(2g\sqrt{\tau\tau'}) \right] \\
 &= \frac{1}{\sqrt{2\pi g}} \left( \frac{1}{\sqrt{s_a}} + \frac{1}{\sqrt{s_b}} \right) \exp \left[ -\frac{g}{2} \left( \frac{1}{\sqrt{s_a}} + \frac{1}{\sqrt{s_b}} \right)^2 \right] \\
 &= \sqrt{\frac{2}{\pi s_* g}} e^{-2g/s_*}, \tag{9}
 \end{aligned}$$

where  $s_a$  and  $s_b$  are the mean partial widths through the two leads  $a$  and  $b$ , and in the last line we use the fact that the distribution depends only on the quantity  $s_*$  defined by

$$\frac{1}{s_*} = \frac{1}{2} \left( \frac{1}{\sqrt{s_a}} + \frac{1}{\sqrt{s_b}} \right). \tag{10}$$

For equal leads,  $s_* = s_a = s_b$ , and we also notice that in general the distribution of  $g$  is just the Porter–Thomas  $\chi^2$

---

<sup>1</sup>For definiteness, we will consider throughout the time-reversal invariant situation. Of course, the calculations can be carried through also in the presence of a magnetic field (the wavefunction intensity distribution for that case has been studied extensively in [11,10]), and all predicted effects are qualitatively similar there.

distribution of one degree of freedom, with mean height  $s_*/4$ .

In this paper we will primarily be interested in the physical case of equal-sized leads (but see also Section III E), however as we will see below the more general expression is a very useful starting point for studying periodic orbit and symmetry effects.

For two generically placed equal-sized leads, we have  $s_a = s_b = s_0$ , and

$$P_{\text{generic}}(g) = \sqrt{\frac{2}{\pi s_0 g}} e^{-2g/s_0}. \quad (11)$$

The properties of this Porter–Thomas distribution are well-known; in particular

$$\langle g \rangle_{\text{generic}} = \frac{s_0}{4} \quad \text{and} \quad \langle g^2 \rangle_{\text{generic}} = 3 \langle g \rangle_{\text{generic}}^2. \quad (12)$$

The ratio of the mean squared height to the square of the mean, also known as the inverse participation ratio (IPR), is the simplest measure of the degree of fluctuation in peak intensities.

We note also that for two leads that are symmetrically placed in a dot with reflection symmetry, the two partial widths  $\Gamma_{an}$  and  $\Gamma_{bn}$  are equal for each resonance  $n$ , and we have  $g_n = \Gamma_{an}/2$ . The peak heights are then again distributed according to a Porter–Thomas law, but with a larger mean height:

$$P_{\text{symmetric}}(g) = \sqrt{\frac{1}{\pi s_0 g}} e^{-g/s_0} \\ \langle g \rangle_{\text{symmetric}} = \frac{s_0}{2}. \quad (13)$$

This factor of 2 enhancement associated with perfect correlation between the two leads, and independent of any short-time dynamical effects, is present already in the case of the horizontal bounce orbit considered in Ref. [3]. We note, however, that the symmetry effect is much less robust than the dynamical effect, requiring the dot potential to be perfectly symmetric to better than a single level spacing (otherwise the even and odd states mix and we recover the generic result of Eq. 11).

Another independent effect, also present in the special example treated in [3], is associated with the placement of one or both leads on the symmetry lines of the system. If both leads are placed on a given symmetry line, as in the case of the horizontal bounce orbit of the stadium, then only the even states produce resonances, leading to half as many peaks as naively expected, but with double the mean height of Eq. 13:

$$\langle g \rangle_{\text{same sym line}} = s_0 \quad [\text{half expected density}]. \quad (14)$$

In a system with two symmetry lines such as the Bunimovich stadium or the Sinai billiard, we may also consider the case of two leads on different symmetry lines. Then only a quarter of the eigenstates produce conductance peaks, the two partial widths are uncorrelated but

each is doubled with respect to the naive expectation  $s_0$ , and we obtain (cf. Eq. 12)

$$\langle g \rangle_{\text{diff sym lines}} = \frac{s_0}{2} \quad [\text{quarter expected density}]. \quad (15)$$

Finally, for just one lead on a symmetry line, only the even wavefunctions contribute with mean partial width  $2s_0$  through the symmetry line lead and  $s_0$  through the other lead; the general expression of Eq. 9 then leads to

$$\langle g \rangle_{\text{one on sym line}} = \frac{2}{(\sqrt{2} + 1)^2} s_0 \approx 0.343 s_0 \\ [\text{half expected density}]. \quad (16)$$

Thus we see that a rich diversity of conductance behavior may be observed simply by considering the placement of one or both leads with respect to the symmetry lines of the system.

## B. One lead on short periodic orbit

We now put aside symmetry considerations and consider a scenario where one of the two conducting leads, say  $a$ , is located on a short (unstable) periodic orbit of the chaotic dot. Then the mean partial width through lead  $a$  is given by  $s_a = s_{a0} S^{\text{smooth}}(E)$  (see Eqs. 3, 5) in an energy range near  $E$ . Taking the two leads to be of equal width,  $s_{a0} = s_b = s_0$ , the effective coupling  $s_*$  becomes energy-dependent:

$$s_*(E) = 4s_0 \left( 1 + 1/\sqrt{S^{\text{smooth}}(E)} \right)^{-2}. \quad (17)$$

Notice that the conductance is always dominated by the more weakly coupled lead: thus near the scarring energies  $S^{\text{smooth}}$  is strongly enhanced and the mean conductance is moderately increased (at most by a factor of 4), while at the antiscarring energies  $S^{\text{smooth}}$  is small, and the mean conductance may be greatly suppressed. Sweeping through energy, one obtains a general expression for the distribution of conductance peak heights:

$$P(g) = \frac{1}{2\pi} \int_0^{2\pi} dE \sqrt{\frac{2}{\pi s_*(E) g}} e^{-2g/s_*(E)}, \quad (18)$$

where  $s_*(E)$  is given by Eq. 17 and  $S^{\text{smooth}}(E)$  by the Fourier transform of Eq. 8. Note that the energy interval corresponding to one oscillation of the scarring envelope is taken as 0 to  $2\pi$ , because we are working in units where  $\hbar = 1$  and the orbit period  $P$  is also normalized to 1. The distribution of Eq. 18 may be computed numerically (see, for example, Fig. 6 below) for various values of the stability exponent  $\beta$  (and lead non-optimality parameter  $Q$ , see Eq. 8). First, however, we obtain some analytic asymptotic results for the strongly scarred case ( $\beta \ll 1$ ), where the deviations from Porter–Thomas behavior are expected to be strongest.

The tail of the distribution  $P(g)$  will be dominated (for any  $\beta$ ) by the peak of the envelope  $s_*(E)$ , which coincides of course with the peak in  $S^{\text{smooth}}(E)$  at  $E = \theta \bmod 2\pi$  (see Eq. 8). The integral may be performed by stationary phase (as in Ref. [11]), to obtain

$$P(g) = \frac{1}{2\pi s_0 g} \sqrt{\frac{A}{B}} e^{-gA/2s_0}, \quad (19)$$

where  $A = 4/s_*^{\text{max}}$  and  $B$  measures the curvature of the envelope at the maximum:  $B = 2\partial^2(s_*^{-1})/\partial E^2$ . Eq. 19 describes the large  $g$  behavior of the conductance peak distribution, where  $A$  and  $B$  are appropriate functions of the instability exponent  $\beta$ . For small  $\beta$  one may simplify further and obtain  $A = 1 + 2\sqrt{\beta/C} + O(\beta)$  and  $B = \frac{1}{2}DC^{-3/2}\beta^{-3/2} + O(\beta^{-2})$ , where  $C \approx 5.24$  and  $D \approx 45.1$  are numerical constants. So finally we obtain the large- $g$  behavior for small  $\beta$ :

$$P(g) = \frac{1}{\sqrt{2\pi}} \frac{C^{3/4} \beta^{3/4}}{D^{1/2} g} e^{-g(1+2\sqrt{\beta/C})/2s_0}. \quad (20)$$

Notice the long tail dominated by the exponential behavior  $\exp(-g/2s_0)$  in the strongly-scarred regime, to be contrasted with the much shorter tail  $\exp(-2g/s_0)$  in the RMT ( $\beta \rightarrow \infty$ ) case.

The asymptotic behavior of Eq. 20 is plotted for instability exponent  $\beta = 1$  as the leftmost dashed curve in Fig. 1, and agrees well with numerical data, represented by a solid curve. Thus, we see that the approximations used in obtaining Eq. 20 are good already for  $\beta = 1$ , even though formally we have used a small- $\beta$  approximation. The Porter-Thomas prediction of RMT (Eq. 11) appears in Fig. 1 as a dotted line for comparison.

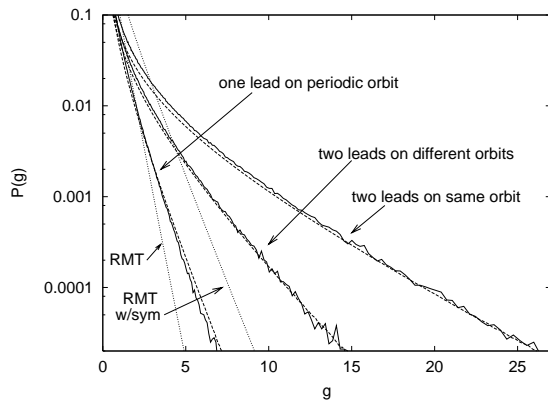


FIG. 1. The tail of the conductance peak height distribution  $P(g)$  is plotted with solid curves for (i) one lead on a periodic orbit with instability exponent  $\beta = 1$ , with the other lead generically placed; (ii) two leads on different orbits, each with instability exponent  $\beta = 1$ , and with in-phase spectral envelopes; and (iii) two leads placed on the same orbit with  $\beta = 1$ . Theoretical predictions, given by Eqs. 20, 35, and 33, respectively, and strictly valid for  $g \gg \beta^{-1} \gg 1$ , are plotted as dashed curves. The mean partial width  $s_0$  through each of the two leads has been set to unity. For reference, the Porter-Thomas prediction of RMT (Eq. 11, to be compared with data sets (i) and (ii)) appears as the lower dotted curve, while RMT modified to include symmetry effects (Eq. 13, to be compared with data set (iii)), is shown as the upper dotted curve. In the dynamics-free limit where  $\beta \rightarrow \infty$ , the data would approach these RMT results.

The predicted increase in the frequency of very small conductance peaks is even more striking. In Ref. [10] it was found that in between the scarring energies  $E = \theta \bmod 2\pi$  where the LDOS  $S^{\text{smooth}}(E)$  is maximized and the antiscarring energies  $E = \theta + \pi \bmod 2\pi$  where it is minimized, the LDOS at the lead follows (for sufficiently small instability exponent  $\beta$ ) the exponential law

$$S^{\text{smooth}}(E) = \frac{2\pi}{\beta} e^{-\frac{\pi}{2\beta}|E-\theta|}. \quad (21)$$

Thus, outside of a small energy window  $|E-\theta| \leq \beta |\log \beta|$  surrounding the energy of maximal scarring, most eigenstates are strongly antiscattered, with mean intensity at the location of the lead being  $S^{\text{smooth}} \ll 1$ . In the strongly antiscattered regime where  $\Gamma_{an}$  is small, we may ignore the partial width through the other lead  $\Gamma_{bn}$  in Eq. 2, and so the conductance  $g_n$  is simply proportional to  $\Gamma_{an} \sim S^{\text{smooth}}(E_n)$ . We then obtain the small- $g$  end of the conductance distribution:

$$P(g) = \frac{2\beta}{\pi^2 g}, \quad (22)$$

which holds formally for  $\exp(-\pi^2/2\beta) \ll g/s_0 \ll \beta \ll 1$ . The constraint  $\exp(-\pi^2/2\beta) \ll g/s_0$  is of no practical significance; we also note that although Eq. 22 becomes exact only in the small  $\beta$  limit, quantitative agreement is already obtained for exponents  $\beta \approx 0.5$ . Eq. 22 should be compared with the generic small- $g$  behavior  $P_{\text{generic}}(g) = \sqrt{2/\pi s_0 g}$  predicted by the Porter-Thomas law (Eq. 11).

The above derivation applies to an optimal lead ( $Q = 0$  in Eq. 8); for a non-optimal lead the result of Eq. 22 is modified only by a  $Q$ -dependent constant, leaving the very distinct  $1/g$  scaling behavior unchanged. The small- $g$  behavior of Eq. 22 is plotted (for instability exponent  $\beta = 0.2$ ) as a dashed line in Fig. 2, and differs greatly from RMT expectations (the latter plotted as a dotted line in the same figure).

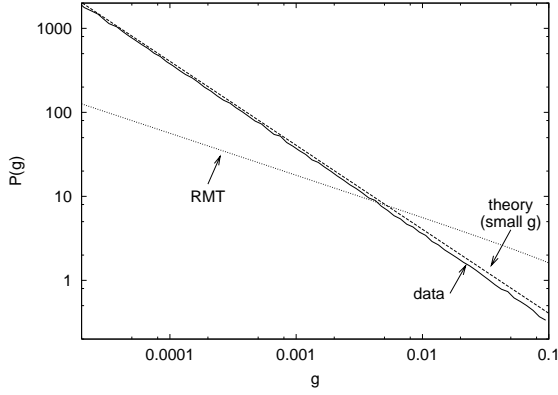


FIG. 2. The small- $g$  part of the peak height distribution  $P(g)$  is plotted on a log-log scale for one lead on an unstable periodic orbit with instability exponent  $\beta = 0.2$  (solid curve). The asymptotic prediction of Eq. 22, valid for  $g \ll \beta \ll 1$  appears as a dashed line of slope  $-1$ . For reference, the RMT prediction of Eq. 11 appears as a dotted line of slope  $-1/2$ . Note the different power-law behavior. Again, the normalization is set so that the mean partial width through each lead is given by  $s_0 = 1$ . The data would be almost identical for the cases where both leads are located on the same periodic orbit with  $\beta = 0.2$ , or where they are located on two in-phase orbits (not shown).

The very large fraction of small conductance peaks clearly must have a significant effect on the moments of the conductance peak distribution. From Eq. 21 we see that only a fraction  $O(\beta|\log \beta|)$  of all energies have  $S^{\text{smooth}} \geq 1$  and at these energies we obtain  $g \sim s_* \sim s_0$  (see Eq. 17). At all other energies we have  $S^{\text{smooth}} \ll 1$  and thus  $g \sim s_* \ll s_0$ . All moments  $k \geq 1$  of the conductance distribution then scale as

$$\left\langle \left( \frac{g}{s_0} \right)^k \right\rangle \sim \beta |\log \beta| \quad (23)$$

for sufficiently small  $\beta$ . In particular, the first two moments are given by

$$\begin{aligned} \langle g \rangle &\approx 0.16\beta |\log \beta| s_0 \\ \langle g^2 \rangle &\approx 0.37\beta |\log \beta| s_0^2. \end{aligned} \quad (24)$$

The inverse participation ratio (IPR) is a useful dimensionless measure of the variation in heights which does not require one to predict theoretically the mean of the distribution:

$$\frac{\langle g^2 \rangle}{\langle g \rangle^2} \approx \frac{14.5}{\beta |\log \beta|}. \quad (25)$$

This result should be compared with an IPR of 3 for the generic Porter–Thomas distribution (see Eq. 12). We see a greatly enhanced fluctuation in peak heights in the case where one of the leads is located in the periodic orbit. We also note that the numerical prefactor of  $\approx 14.5$  is valid for an optimally placed lead ( $Q = 0$  in Eq. 8).

In general there is an additional prefactor which is an easily computable analytic function of the width of the Gaussian lead mode and of the monodromy matrix of the periodic orbit, but the important scaling behavior, i.e. the increase as  $1/\beta |\log \beta|$  of the fluctuations for small  $\beta$ , is unchanged.

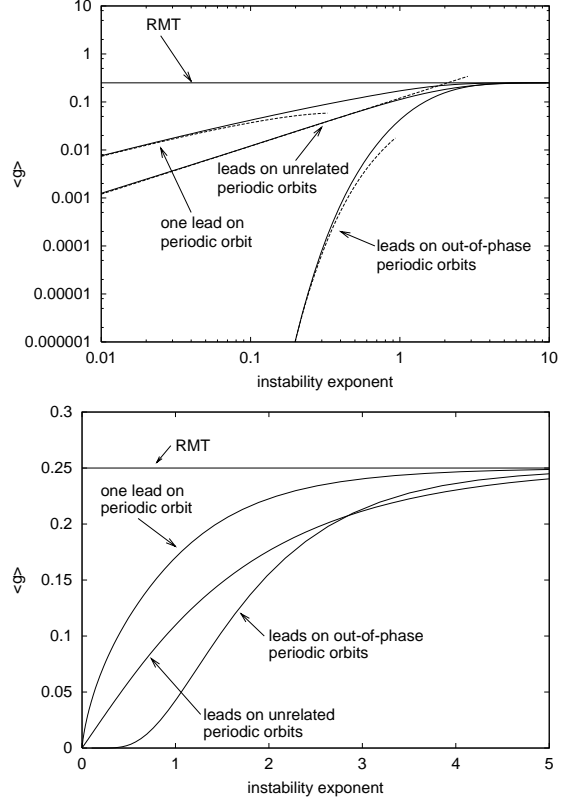


FIG. 3. The mean conductance peak height  $\langle g \rangle$  is plotted as a function of the instability exponent  $\beta$ . Three cases are shown: (i) one lead on an orbit of exponent  $\beta$ , with the other lead placed generically; (ii) two leads on unrelated orbits each having exponent  $\beta$ ; and (iii) two leads on out-of phase periodic orbits with exponent  $\beta$ . For two leads on the *same* periodic orbit, the mean conductance follows the RMT prediction (with symmetry), and is independent of the exponent  $\beta$ . (Top) Solid curves are exact; dashed curves are asymptotic forms valid for  $\beta \ll 1$ , given by Eqs. 24, 39, and 37, respectively. In the dynamics-free limit  $\beta \rightarrow \infty$ , all curves approach the RMT prediction 0.25, which is shown on the graph for comparison. (Bottom) Same data is shown for moderate to large values of the exponent  $\beta$ , where the asymptotic forms are not applicable.

The numerically computed mean conductance  $\langle g \rangle$  for one lead on an orbit of instability exponent  $\beta$  appears in Fig. 3 as a function of  $\beta$  (solid curve). We observe significant deviations from the RMT value of 0.25 (Eq. 12, where  $s_0$  has been set to unity) for  $\beta$  as large as 2.0, while for larger values of  $\beta$  the RMT limit is approached. The dashed curve in Fig. 3(top) shows the asymptotic prediction of Eq. 24, which is observed to agree well with the

exact results only for very small  $\beta$ .

The asymptotic behavior of Eq. 25 appears in Fig. 4(top) as a dashed curve, and can be compared with numerical data, which is plotted as a solid line. We observe that the approximations leading to Eq. 25 do not lead to a quantitatively correct answer until we reach the very weakly unstable  $\beta \ll 0.1$  regime. On the other hand, strong enhancement of the IPR compared to the RMT value of 3 is already clearly visible even near the moderate exponent  $\beta = 1$ , where the IPR is observed to be almost twice the RMT prediction. Fig. 4(bottom) shows the same calculation, focusing in on the IPR behavior for moderate values of  $\beta$ , where the approximations leading to Eq. 25 do not apply.

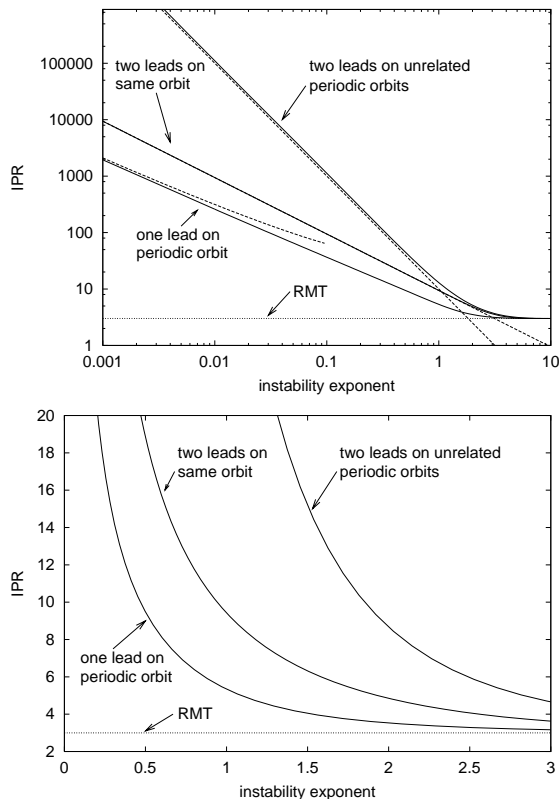


FIG. 4. The IPR (ratio of mean squared conductance peak height to the square of the mean) is plotted as a function of the instability exponent  $\beta$  of the periodic orbit. Three cases are shown: (i) one lead on an orbit with exponent  $\beta$ , with the other lead placed generically; (ii) two leads on unrelated periodic orbits, both with exponent  $\beta$ ; and (iii) two leads on the same periodic orbit. The RMT prediction of 3 is shown as a dotted line for reference; all solid curves converge to the RMT value in the  $\beta \gg 1$  regime where the orbit ceases to be important. (Top) The solid curves are exact numerical results, while the dashed curves give the asymptotic  $\beta \ll 1$  predictions of Eqs. 25, 42, and 32. (Bottom) Same data is shown for moderate values of  $\beta$ , where the asymptotic forms are not applicable.

The analysis in this subsection easily generalizes to the

case where the lead located on the periodic orbit also lies on a symmetry line of the system. As discussed in the previous subsection, the odd eigenstates do not then produce resonance peaks, while for the even states we use  $s_{a0} = 2s_0$ , and thus

$$s_*(E) = 4s_0 \left( 1 + 1/\sqrt{2S^{\text{smooth}}(E)} \right)^{-2}. \quad (26)$$

instead of the expression given by Eq. 17.

### C. Leads on same periodic orbit, or on orbits related by symmetry

We now proceed to consider more generally the case discussed by Narimanov et al. [3], where the two leads are either located on the same periodic orbit, or are located on orbits related by symmetry. First, we notice that if the two leads themselves are related by a symmetry, then the two wavefunction intensities and thus the two partial widths are identical for each resonance, just as in the discussion leading to Eq. 13 in the generic case. Less trivially, let us consider two leads located on the same orbit but not related by a symmetry (for example, one may consider the horizontal bounce in a deformed stadium billiard lacking a left-right symmetry, and two leads placed at either end of the horizontal bounce orbit). If the Gaussian packet corresponding to the transverse mode in lead  $b$  were related to the Gaussian packet associated with lead  $a$  by time evolution in the closed system, i.e.

$$|\phi_b\rangle = e^{-i\hat{H}t/\hbar} |\phi_a\rangle \quad (27)$$

for some  $t$ , then  $|\phi_a\rangle$  and  $|\phi_b\rangle$  would have identical local densities of states,  $|\langle \Psi_n | \phi_a \rangle|^2 = |\langle \Psi_n | \phi_b \rangle|^2$ , and thus once again  $\Gamma_{an} = \Gamma_{bn}$  for each resonance  $n$ .

More generally, even though the centers of the Gaussians  $|\phi_a\rangle$  and  $|\phi_b\rangle$  must be related by time evolution if they lie on the same orbit, the time-evolved version of  $|\phi_a\rangle$  may have a different aspect ratio or phase space orientation from  $|\phi_b\rangle$ . In Ref. [15] it was found, however, that for any two *optimally* shaped leads, the two local densities of states become almost identical in the limit of small instability exponent  $\beta$ . Furthermore the *minimum* possible correlation between the two partial widths was shown to be 0.94 even for  $\beta$  as large as 2.3 (corresponding to a classical stretching factor  $e^\beta = 10$ ), and this correlation becomes even stronger for smaller  $\beta$ , so that for all practical purposes in the regime where scarring effects are important we may take  $\Gamma_{an} \approx \Gamma_{bn}$  for any two optimally oriented leads.

In the case where either of the leads  $a$  or  $b$  are not optimally shaped so as to be aligned with the stable and unstable manifolds of the periodic orbit, we have the more general situation

$$\begin{aligned}\Gamma_{an} &= C_a(\alpha r_n + (1 - \alpha)r_{an})S^{\text{smooth}}(E_n) \\ \Gamma_{bn} &= C_b(\alpha r_n + (1 - \alpha)r_{bn})S^{\text{smooth}}(E_n),\end{aligned}\quad (28)$$

where we normally consider equally-coupled leads  $C_a = C_b$  as before, and  $r_n$ ,  $r_{an}$ , and  $r_{bn}$  are independent random (Porter–Thomas) variables. The parameter  $0 < \alpha < 1$  may be determined in terms of the linearized time evolution of the two wavepackets around the orbit [15]. In the weakly correlated regime  $\alpha \rightarrow 0$ , the behavior becomes identical to that of two leads on different orbits but having in-phase short-time envelopes  $S^{\text{smooth}}(E)$ . See Section III D below for a detailed discussion of that situation; for now we restrict ourselves to the strongly correlated case  $\alpha \approx 1$ . We also note that all results valid for two leads on the same orbit are obviously valid also for leads on two orbits related by symmetry (e.g. for the two V-shaped orbits of the stadium).

In the case  $\alpha \approx 1$ , valid for two nearly optimal leads located on a weakly unstable orbit, the conductance peak height distribution reduces simply to the distribution of wavefunction intensities on a short periodic orbit. This distribution has been studied previously [11,10] in the absence of time reversal symmetry (i.e. in the presence of a magnetic field); here we need to develop parallel results for the case where a magnetic field is absent and the wavefunctions are therefore real.

We begin with the moments of the distribution. At any given energy, the peaks heights  $g$  are distributed according to a Porter–Thomas distribution as in Eq. 13, but the mean height ( $s_0/2$  in the generic case) must be generalized to  $S^{\text{smooth}}(E)s_0/2$  (see Eq. 5). The moments of  $P(g)$  are then given by

$$\langle g^q \rangle = \left\langle (S^{\text{smooth}}(E))^q \right\rangle \left\langle \left( r_n \frac{s_0}{2} \right)^q \right\rangle, \quad (29)$$

where the average in the first factor is over energies  $E$  and in the second factor  $r_n$  is distributed as the square of a Gaussian variable with variance 1. For generically located (though symmetrically placed) leads,  $S^{\text{smooth}}(E) = 1$  independent of  $E$  and we recover the result of Eq. 13. We notice also that  $\langle S^{\text{smooth}}(E) \rangle = 1$  by normalization, so the mean conductance peak height is given by

$$\langle g \rangle_{\text{leads on same orbit}} = \frac{s_0}{2}, \quad (30)$$

when both leads are located on the same orbit, independent of the stability of the orbit. This is in contrast with our finding in the previous subsection (Eq. 24) that the mean conductance is suppressed when only one lead is located on a short orbit. Furthermore, the mean squared intensity in this case is *enhanced* compared to the generic value:

$$\begin{aligned}\langle (S^{\text{smooth}}(E))^2 \rangle &= \sum_t |A^{\text{short}}(t)|^2 \\ &= \sum_m \frac{1}{\cosh \beta m} \\ &\approx \frac{\pi}{\beta},\end{aligned}\quad (31)$$

where in the first line we have used the property of Fourier transforms (recalling Eq. 6), in the second line we have substituted from Eq. 8 the optimal ( $Q = 0$ ) form of the short-time autocorrelation function, and in the third line we have taken the strong scarring ( $\beta \ll 1$ ) limit. Then we obtain

$$\langle g^2 \rangle \approx 3 \frac{\pi}{\beta} \langle g \rangle^2. \quad (32)$$

The validity of this result is confirmed in Fig. 4(top), where the IPR ( $\langle g^2 \rangle / \langle g \rangle^2$ ) is plotted as a function of the instability exponent  $\beta$ . The data for two leads on the same orbit appears there as the middle solid curve, which for  $\beta \leq 2$  agrees very well with the asymptotic prediction of Eq. 32 (represented by a dashed line of slope  $-1$ ). The behavior of the same quantity for larger exponents  $\beta$  can be seen in Fig. 4(bottom), where we observe that already for  $\beta = 1$  the size of peak height fluctuations is three times the RMT expectation, and that deviations from RMT are noticeable even for  $\beta$  as large as 3.

Thus the IPR can greatly exceed the RMT value of 3 and grows as the orbit on which the leads are placed becomes less unstable. This suggests that there should be an excess of both very large and very small peaks as compared with the mean (qualitatively similar to the result (Eq. 25) for only one lead on a periodic orbit). Indeed one can study the tail of the  $P(g)$  distribution in a way completely analogous to the calculation in the previous subsection (and to the similar calculation in [11] for the non-TRS case). From Eq. 19, we obtain (using  $s_*(E) = 2s_0 S^{\text{smooth}}(E)$  instead of the corresponding form Eq. 17 appropriate for only one lead on a periodic orbit)

$$P(g) = \sqrt{\frac{C}{2\pi^2 D}} \beta e^{-\beta g / C s_0}, \quad (33)$$

valid for small  $\beta$  and large  $g$ . As in Eq. 20, we see a much slower exponential decay in the tail than that predicted by RMT, but in this case the exponent is strongly  $\beta$ -dependent and so the tail becomes ever longer as  $\beta \rightarrow 0$ . Eq. 33 (for  $\beta = 1$ ) appears in Fig. 1 as the rightmost dashed curve, and follows very well the exact numerical result, which is shown as a solid curve. We see that the asymptotic prediction of Eq. 33 is already very good even for the moderate exponent  $\beta = 1$ , while the RMT prediction (Eq. 13) is completely wrong in the tail (compare with dotted curve), even after symmetry effects are included.

This strong enhancement in the number of very large conductance peaks is balanced by a corresponding increase in the number of very small conductance peaks: the small- $g$  part of the distribution is given again by Eq. 22, exactly as in the case of only one lead on a periodic orbit. The small- $g$  data for two leads on the same orbit is not shown here, but appears very similar to the case already plotted in Fig. 2 for only one lead on a short orbit.



The expressions obtained in this subsection need, of course, to be modified for situations where one of both leads are located on a symmetry line of the system. The necessary modifications are completely analogous to those discussed in the previous two subsections, and we do not go into the details here.

#### D. Leads on different periodic orbits

We now arrive at perhaps the most interesting situation, where the two leads are located on distinct (not symmetry-related) periodic orbits of the classical system. This situation is particularly interesting because a very rich diversity of behavior may be obtained depending on the relative phase between the classical actions, in units of  $\hbar$ , of the two orbits. For definiteness and for simplicity of presentation, we will focus on the case where two orbits have equal stability exponents  $\beta$ , though the qualitative results obviously do not depend on this assumption. We also take the periods of the two orbits to be approximately equal, instead of being related by some other simple fraction like  $1/2$  or  $2/3$  (see the end of this subsection for a discussion of what happens in the case where the two orbit lengths are not at all simply related). Then the LDOS envelopes  $S^{\text{smooth}}(E)$  at the two leads are identical oscillatory functions of energy, shifted with respect to each other by some phase  $\delta\theta$  (see Eqs. 6, 8).

For  $\delta\theta = 0$ , we obtain two in-phase envelopes, and recover the  $\alpha = 0$  situation of identical smooth envelopes with uncorrelated fluctuations under the envelopes. This scenario was mentioned already in the previous subsection (Eq. 28), but the discussion there was postponed until now. We recall that for two uncorrelated partial widths with the same mean, the distribution of conductances is Porter–Thomas (Eq. 11), just as in the perfectly correlated case (Eq. 13), but the mean conductance in the uncorrelated case is only half as large as in the correlated case. This argument applies of course independently at each energy, so even after averaging over energy we obtain the same distribution of conductances as in the previous subsection, but with the mean value shifted by a factor of 2. To summarize, the mean is given by

$$\langle g \rangle_{\text{leads on in-phase orbits}} = \frac{s_0}{4} \quad (34)$$

(cf. Eq. 30), while the IPR and the small- $g$  part of the distribution (Eqs. 32, 22), respectively, remain unchanged from the previously considered case. The tail of the conductance peak distribution becomes

$$P(g) = \sqrt{\frac{C}{2\pi^2 D}} \frac{\beta}{g} e^{-2\beta g/Cs_0}. \quad (35)$$

The result of Eq. 35 is plotted for  $\beta = 1$  as the middle dashed curve in Fig. 1, and is observed to agree well with the numerical calculation, given by the corresponding solid curve. We again note that the asymptotic form

of Eq. 35 works quantitatively even though  $\beta$  in our case is not small; furthermore the tail of the peak height distribution  $P(g)$  again differs greatly from the RMT prediction (leftmost dotted curve in the same figure).

We now consider two envelopes  $S^{\text{smooth}}$  that are not in phase with each other. From Eq. 21 we know that each envelope falls off exponentially away from its peak, and we also know from Eq. 2 that when the two local densities of states are unequal, the conductance is always dominated by the more weakly-coupled lead (smaller  $S^{\text{smooth}}$ ). The maximum conductance then occurs at energies where  $S_a^{\text{smooth}} \approx S_b^{\text{smooth}}$ . This maximum occurs at  $E = (\phi_a + \phi_b)/2 \bmod 2\pi = \phi_a + \delta\phi/2 \bmod 2\pi$ , at which energy  $S_a^{\text{smooth}} = S_b^{\text{smooth}} = (2\pi/\beta) \exp(-\pi\delta\phi/4\beta)$ . The *maximum* possible conductance peak height is therefore very strongly suppressed compared with the RMT prediction:

$$g_{\text{out of phase orbits}}^{\text{max}} \sim \frac{s_0}{\beta} e^{-\pi\delta\phi/4\beta}, \quad (36)$$

where the out-of-phase parameter  $\delta\phi$  should be taken between 0 and  $\pi$ . We also note that the fraction of energy space at which conductances this large are attained scales as  $\beta$  because of the exponential falloff in Eq. 21; thus the *mean* conductance peak height scales as

$$\langle g \rangle_{\text{out of phase orbits}} \sim s_0 e^{-\pi\delta\phi/4\beta}, \quad (37)$$

suppressed by an exponential factor from the generic expectation of Eq. 12. The most dramatic effect arises of course when the two envelopes are out of phase by exactly  $\pi$  in the energy region of interest. There we have

$$g^{\text{max}} \sim \frac{s_0}{\beta} e^{-\pi^2/4\beta} \quad \langle g \rangle \sim s_0 e^{-\pi^2/4\beta}. \quad (38)$$

An exact numerical calculation for  $\langle g \rangle$  is plotted as the lowest solid curve in Fig. 3(top), and is observed to approach the asymptotic prediction of Eq. 38 for small  $\beta$ , while for large  $\beta$  it of course tends to the RMT prediction of 0.25. Again, Fig. 3(bottom) shows in more detail the behavior for moderate-to-large values of  $\beta$ .

This situation described by Eq. 38 may be obtained in one of the following two ways. One possibility is to take two orbits of the same period but different Maslov phases, resulting in out-of phase behavior at all energies. Alternatively one may consider two orbits of only approximately equal period; then the two oscillating envelopes move in and out of phase with each other as one sweeps through energy by adding electrons to the dot.

In the scenario of leads placed on two orbits with irrationally-related periods, we can also imagine collecting statistics over an energy window wide enough to include both in-phase and out-of-phase behavior. We see in this case that the peak height will always be exponentially suppressed except at those energies where *both* LDOS envelopes  $S_a^{\text{smooth}}(E)$  and  $S_b^{\text{smooth}}(E)$  are near their respective maxima, i.e. where the wavefunction is scarred simultaneously at each of the two leads. Since in

each envelope the bumps corresponding to scarred wavefunctions have width  $O(\beta)$  compared with the spacing between the bumps, and since the bumps in  $S_a^{\text{smooth}}(E)$  and  $S_b^{\text{smooth}}(E)$  are now assumed to be uncorrelated, we find that a fraction  $O(\beta^2)$  of all wavefunctions give rise to substantial peaks, of height  $O(\beta^{-1}s_0)$ . Then the mean conductance peak height scales for small  $\beta$  as

$$\langle g \rangle_{\text{uncorrelated orbits}} \sim \beta s_0, \quad (39)$$

and the higher moments of the distribution behave similarly:

$$\langle g^k \rangle_{\text{uncorrelated orbits}} \sim \beta^{2-k} s_0^k; \quad (40)$$

$$\langle g^{\text{max}} \rangle_{\text{uncorrelated orbits}} \sim \beta^{-1} s_0; \quad (41)$$

Again, we may measure the fluctuation in conductance peak heights by taking the ratio of the mean squared peak height to the square of the mean (IPR). This shows very strong deviations from RMT expectations:

$$\left( \frac{\langle g^2 \rangle}{\langle g \rangle^2} \right)_{\text{uncorrelated orbits}} \sim \beta^{-2}. \quad (42)$$

Because both leads must be scarred to obtain appreciable conductance, the fluctuation in conductance peak heights is much stronger here than in the case of only one lead on a periodic orbit (Eq. 25) or even in the case of two leads on the same orbit (Eq. 32).

The mean conductance peak height  $\langle g \rangle$  for leads on two unrelated periodic orbits of instability exponent  $\beta$  is plotted as a function of  $\beta$  as the labeled solid curve in Fig. 3(top), where the  $\beta \ll 1$  asymptotic prediction of Eq. 39 appears as a dashed line. The behavior for larger  $\beta$  again can be seen in Fig. 3(bottom). Similarly, the IPR for this case can be found plotted numerically by the correspondingly labeled solid curves in Fig. 4(top and bottom); again for small  $\beta$  the result agrees with the asymptotic prediction of Eq. 42 (Fig. 4(top); dashed line).

### E. Leads with unequal coupling

We have been focusing throughout on the simple and experimentally motivated case of two equal-sized leads; however all of the discussion and calculations in this section generalize in a very straightforward way to a scenario with unequally coupled leads. Qualitatively, the main observation that should be added to the previous discussion is that the lead which is more weakly coupled naturally has a stronger effect on the conductance peak heights and their distribution, and the location of the more weakly coupled lead relative to classical structures is most important in understanding the conductance behavior.

A particularly interesting case to consider is where one of the leads, say  $b$ , is coupled to the dot much more strongly than the other lead, so  $C_a \ll C_b$  in Eq. 3. Then Eq. 2 reduces to  $g_n \approx \Gamma_{an}$ , and the conductance depends only on the intensity of the wavefunction near lead  $a$ . Since  $s_b \gg s_a$ , Eq. 10 becomes  $s_* = 4s_a$ , and we obtain behavior identical to that observed previously for two symmetrically placed leads (Section III C), except that  $s_0$  must be replaced everywhere by  $2s_a$ . Thus, for example, we obtain

$$\langle g \rangle = s_a \quad (43)$$

(independent of the location of lead  $a$ ), while the IPR is given by Eq. 32 if lead  $a$  is located on an orbit of instability exponent  $\beta \ll 1$ . The tail of the peak height distribution becomes

$$P(g) = \sqrt{\frac{C}{2\pi^2 D}} \frac{\beta}{g} e^{-\beta g/2C s_a}. \quad (44)$$

Of course, for these results to be valid the coupling to lead  $a$  must be weaker than the coupling to  $b$  even near energies where lead  $a$  is scarred; assuming  $b$  is placed generically, this means  $C_a \ll \beta C_b$ . If this condition is satisfied, the unequal-leads experiment may present an practical alternative to trying to ensure that both leads are centered on a periodic orbit.

## IV. NUMERICAL TESTS

We now proceed to look at the implications of the results of the previous section for a specific chaotic system, namely the Bunimovich stadium. This consists of two semicircular endcaps of radius 1, attached to either side of a rectangle of dimension  $2 \times 2\gamma$ . The system reduces to a circle for  $\gamma = 0$ ; maximum chaos is attained at  $\gamma = 1$ . We will focus mostly on the  $\gamma = 1$  special case, though scar effects are stronger at smaller values of  $\gamma$  (as the periodic orbit instability exponents  $\beta$  become smaller).

The (Dirichlet) wavefunctions of a billiard system such as the stadium can be obtained by the plane wave method, where at each  $k_F$  one constructs the linear combination of plane waves that minimizes the integral of  $|\psi|^2$  along the boundary, and then picks out those values of  $k_F$  where this integral dips down towards zero. Of course, the integral never becomes strictly zero because of the finite number of plane waves used at any given  $k_F$ ; however, it can easily be checked that identifying all the sharp minima in the boundary integral with eigenvalues produces the right density of states, as predicted by the Weyl law and higher-order corrections. For each wavefunction obtained using this method, we can compute the partial widths through each of the two leads via Eq. 3, by simply integrating the normal derivative of the wavefunction at the boundary, multiplied by the (Gaussian)

lowest transverse mode in the lead (Eq. 4). The conductance peak height associated with that resonance is then easily obtained using Eq. 2.

We begin by considering two leads symmetrically placed on the two semicircular endcaps. As we have seen above in Eq. 30, the mean conductance peak height should be independent of classical structures near the lead location, and this behavior is indeed observed when averaging over the energy range  $300 < k_F < 350$ . However, the fluctuation in peak heights, as measured for example by the mean squared height, is expected to depend strongly on whether the leads are located on a short periodic orbit that is normally incident at the location of the lead (Eq. 32).

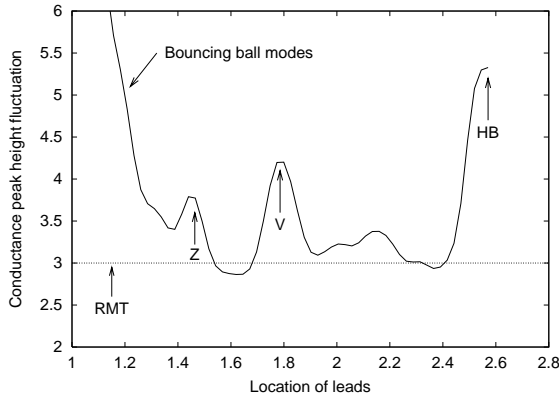


FIG. 5. The IPR of the conductance peak heights (mean squared peak height divided by the square of the mean) is plotted as a function of the distance of each lead from the center of the straight segment in a stadium billiard. The two leads are placed symmetrically on the two semicircular caps, and have width  $\sigma = 1.2/\sqrt{k_F}$ , which corresponds to  $\approx 3.5\lambda_F$  in the energy range considered ( $300 < k_F < 350$ ). The amount of fluctuation is significantly enhanced when the leads are located on unstable periodic orbits, as compared with the RMT prediction of 3. The locations of the three shortest periodic orbits having normal incidence on the semicircular endcaps (horizontal bounce, V-shaped orbit, and Z-shaped orbit) are marked on the plot. On the horizontal axis,  $\gamma = 1.0$  corresponds to the end of the straight segment, and  $\gamma + \pi/2 \approx 2.57$  corresponds to the middle of the circular endcap.

This qualitative expectation is confirmed in Fig. 5, where we clearly see that the mean squared peak height is strongly enhanced over the RMT value whenever the leads (of width  $\sigma = 1.2/\sqrt{k_F} \approx 3.4\lambda_F$ ) are located on a short periodic orbit. Furthermore, the three shortest (and least unstable) orbits in the stadium having normal incidence on the endcaps are the horizontal bounce (HB), the V-shaped orbit, and the Z-shaped orbit, in that order, and these are seen to correspond precisely to the three most pronounced peaks in the plot. We note that the periodic orbit length (as well as the instability exponent  $\beta$ ) must be measured by identifying the four quadrants of the stadium billiard, due to symmetry:

thus, for example, the length of the horizontal bounce orbit is  $2 + 2\gamma = 4$ . Looking at the length of the orbit (and instability exponent) in the full billiard, we would be led to underestimate the true importance of scarring effects.

Notice that the leads are always located on the upper half of the stadium, equidistant from the center point of the upper straight segment. Thus, for both the horizontal bounce and the V-shaped orbit, the two leads happen to be on the same orbit, while in the case of the Z-shaped orbit, the leads would be placed on distinct orbits that were related by symmetry. As noted above, this difference has no effect on the conductance behavior.

We also see a strong increase in peak height fluctuations as the leads approach the edge of the straight segment. This is not surprising since the quantum behavior there is strongly influenced by bouncing-ball and near-bouncing-ball modes [16]. For a lead located on the straight segment of the boundary, the IPR will tend to infinity in the high-energy limit. In other words, a smaller and smaller fraction of all modes will give rise to appreciable conductance in this limit.

To understand the conductance behavior at a quantitative level, we focus in on the most pronounced peak in Fig. 5, corresponding to leads located on the horizontal-bounce orbit, i.e. centered opposite to one another on the two semicircular endcaps. For  $\gamma = 1$ , the system previously considered in [3], the mean squared peak height is observed to be enhanced by a factor of 1.78 over the RMT prediction, as compared with an expected enhancement of 1.81 coming from Eq. 32, where we have used the value  $\beta = 1.76$  appropriate to this orbit. [We note that for the value of the lead width  $\sigma$  given above, the lead shape is close enough to being optimal that we may ignore corrections associated with non-zero parameter  $Q$  in Eq. 8, discussed above.] Such close agreement is surely accidental, as one expects deviations due to the finite number of conductance peaks being sampled, as well as systematic finite-energy errors associated with corrections to the semiclassical approximation and also with the presence of non-random bouncing ball and whispering gallery modes. Indeed, looking at leads centered on the horizontal bounce orbit in the  $\gamma = 1/2$  stadium, and also at leads centered on the V-shaped orbit in the original  $\gamma = 1$  stadium, we find in each case that the observed mean squared peak height is about 10% lower than the predicted value (but still much higher than the RMT expectation). See Table I for details. In all three cases, the measured value of  $\langle g^2 \rangle / \langle g \rangle^2$  is easily distinguishable from the IPR value of 3.

lead locations	$\langle g \rangle$			$\langle g^2 \rangle / \langle g \rangle^2$		
	actual	theory	RMT	actual	theory	RMT
both on HB	0.50	0.50	0.50	5.33	5.43	3.00
both on HB	0.50	0.50	0.50	6.44	7.17	3.00

$(\gamma = 0.5)$						
both on V	0.50	0.50	0.50	4.23	4.80	3.00
HB and generic	0.21	0.22	0.25	3.70	3.73	3.00
HB and V	0.20	0.19	0.25	4.11	4.50	3.00
generic (symmetric)	0.50	0.50	0.50	3.02	3.00	3.00

TABLE I. Mean and mean squared conductance peak heights are shown for several lead locations in the stadium billiard, and are compared with scar theory as well as with RMT. Unless stated otherwise,  $\gamma = 1$  is used for the shape of the billiard (see text above). We consider two cases where both leads are located on the same (horizontal bounce) orbit, and one where they are located on symmetry-related (V-shaped) orbits. In addition, scenarios are shown where one lead is located on the horizontal bounce, while the other is placed either on the V-shaped orbit or at a generic location ( $q = 2.3$  in the coordinates of Fig. 5). For reference, we also show a calculation where the two leads are symmetrically placed at a generic location; there we see that good agreement with RMT is obtained.

The first two moments of  $P(g)$ , as shown in Table I, provide useful and concise information about the distribution of conductance peak heights  $g$ , and can be easily used to distinguish generic lead locations from the case of leads located on a whost periodic orbit. More complete information is of course contained in the full distribution, as shown in Fig. 6. [The distributions there are shown as cumulative probabilities  $\int_g^\infty dg' P(g')$ , so as to reduce the effect of statistical noise.] We see, for the case of both leads located on the HB orbit, a long tail (Fig. 6(bottom), top solid curve) in good quantitative agreement with the prediction of scar theory (dashed curve). We also see in Fig. 6(top, solid curve, second from top) the increased number of small conductance peak heights as compared with RMT, and again in very good agreement with scar theory predictions (accompanying dashed curve).

We recall also (from Section III E) that, up to an overall scaling factor of 2, exactly the same distribution would be obtained for only one lead located on a short orbit of the stadium, with the other, much more strongly coupled, lead located at a generic location.

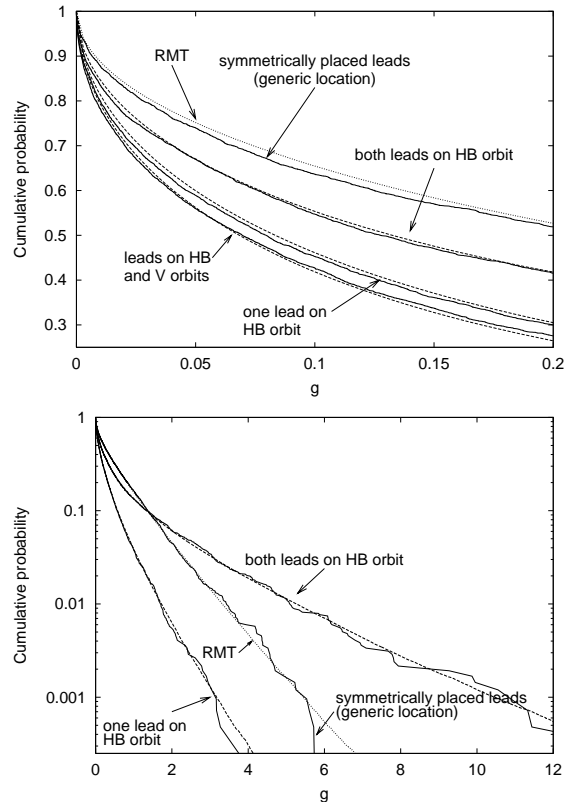


FIG. 6. The cumulative probability  $\int_g^\infty dg' P(g')$  of having conductance peak height greater than  $g$  in a stadium billiard with two leads is plotted for several lead locations, illustrating the various scenarios considered in the previous section: (i) both leads located on the horizontal bounce orbit, (ii) one lead on the HB orbit and the other at a generic location, (iii) one lead on the HB orbit and the other on the V-shaped orbit (top figure only), and (iv) the two leads symmetrically placed at a generic location. The solid curves represent stadium data, while the dashed curves represent scar theory predictions (Eq. 18, etc.); for the case of generically placed leads, the scar theory prediction coincides with RMT (shown as a dotted curve). The axes are scaled so as to focus on the tail of the distribution in the bottom figure and the head in the top figure.

We may also consider attaching two leads to the stadium so that only one of them is located on a short orbit (compare Section III B). We see from Table I that in this case the mean conductance is reduced as compared with RMT, while the ratio of the mean square to the square of the mean is enhanced, in agreement with the predictions. The full probability distribution for this case also appears in Fig. 6 (appropriately labeled solid curves, top and bottom), where we see a very noticeably shortened tail as well as an excess of small intensities, as compared with the previously considered case (namely, both leads on the HB orbit). The distribution, in the head, body, and tail, is in good agreement with the theoretical prediction of Eq. 18.

Finally, the next-to-last line in Table I shows the conductance behavior for the case of two leads found on unrelated short orbits, in this case the horizontal bounce and the V-shaped orbit. Both the suppression of the mean conductance and the enhancement of conductance fluctuations (as compared with RMT) are observed, as predicted in Section III D. However, the size of the effect is  $\approx 20\%$  smaller than predicted by the theory. This difference may easily be ascribed to finite-energy effects considered above, in conjunction with statistical fluctuations. The head of the distribution is shown in Fig. 6(top, lowest solid curve), and follows the scar theory prediction, which again appears as a dashed curve. The tail of the distribution would overlap the one discussed in the immediately preceding paragraph (one lead on HB, with the other lead generic), and is not shown.

Finally, the last line in Table I shows the moments of the conductance peak height distribution for generically placed leads, which are seen to agree very well with RMT statistics. The distribution for this case is also plotted in Fig. 6(top and bottom), and as expected it follows the RMT prediction.

## V. CONCLUSION

In this paper we have studied the statistical properties of transmission through a weakly open chaotic cavity. We

have seen that RMT does a very good job in describing these properties when the leads are located far from classically important structures. However, the random-wave hypothesis needs to be modified for a quantitatively accurate description of the transmission process when one or both leads are located near a classically important structure, such as an unstable periodic orbit. The unstable periodic orbits have a strong effect on the distribution of conductance peak heights, even in the limit where the dwell time inside the dot becomes very large compared to the Lyapunov scale on which classical decay away from the unstable orbits takes place. This implies that short-time classical dynamics leaves its imprint on quantum behavior at arbitrarily long time scales, even though at these scales the classical dynamics loses all memory of its short time behavior. We emphasize that the effect considered in this paper is unrelated to direct processes, and arises purely from quantum mechanical interference.

We have also seen that scar-like effects on conductance behavior in a quantum dot are robust, and that statistical predictions about the distribution of peak heights can be made even though we do not have enough information to compute the individual resonances of the system, either quantum mechanically or semiclassically. This means in particular that changes in the mean field which arise as electrons are added to the dot may not significantly effect the statistical properties of the conductance, even though they completely destroy all predictive power for individual resonant wavefunctions. Similarly, electron-electron interactions are expected to make the single-particle picture irrelevant for the purpose of predicting individual resonances or the spacing distribution, but should not affect the statistical properties of the conductance as long as the interaction mean free path is larger than the ballistic path associated with one crossing of the dot.

The mean conductance, higher moments, and the full distribution of peak heights may all be easily computed using scar theory ideas, for the various scenarios considered in this paper. These include a single lead located on a short orbit, two leads located on distinct orbits, or two leads located on the same orbit. The last scenario was seen to be mathematically equivalent both to two leads located on orbits related by symmetry, and also to a situation of unequally-coupled leads, where only the weakly coupled lead needs to be located on a short orbit. All these scenarios may be relevant to different experimental setups.

Experimentally, it is of course much easier to change the classical dynamics inside the dot (either by adjusting the classical geometry or by turning on a strong magnetic field) than it is to sweep through different locations of the lead. Thus, one may consider a situation where the lead locations are fixed but the classical dynamics is changed by adjusting either a voltage or a magnetic field strength. Changes in the peak height fluctuations are then predicted when the adjustable parameter passes through values which cause a periodic orbit to hit one or both of the leads.

In this paper we have not considered peak height correlations [3] or the effect of finite temperature on conductance peak heights; both of these are important effects which have been addressed previously by other authors. We have emphasized the crucial importance of including dynamical information for a quantitative understanding of conductance peak heights in a quantum dot. We also note that similar dynamical effects should be present in other physical situations where tunneling in or out of a chaotic well is important, and dynamical structures inside the well (such as unstable periodic orbits) will influence the distribution of coupling strengths between the well and the outside world. Work along these lines involving tunneling into a smooth potential well is currently under development.

## VI. ACKNOWLEDGMENTS

This research was supported by the DOE under Grant DE-FG-06-90ER40561.

- 
- [1] M. A. Kastner, *Rev. Mod. Phys.* **64**, 849 (1992).  
 [2] H. Grabert and M. H. Devoret, *Single Charge Tunneling: Coulomb Blockade Phenomena in Nanostructures* (Plenum, New York, 1992).  
 [3] E. E. Narimanov, N. R. Cerruti, H. U. Baranger, and S. Tomsovic, *Phys. Rev. Lett.* **83**, 2640 (1999).  
 [4] T. S. Monteiro, D. Delande, A. J. Fisher, and G. S. Boebinger, *Phys. Rev. B* **56**, 3913 (1996); E. E. Narimanov, A. D. Stone, and G. S. Boebinger, *Phys. Rev. Lett.* **80**, 4024 (1998); E. B. Bogomolny and D. C. Rouben, *Europhys. Lett.* **29**, 7 (1995).  
 [5] R. A. Jalabert, A. D. Stone, and Y. Alhassid, *Phys. Rev. Lett.* **68**, 3468 (1992); V. N. Prigodin, K. B. Efetov, and S. Iida, *Phys. Rev. Lett.* **71**, 1230 (1993); E. R. Mucciolo, V. N. Prigodin, and B. L. Altshuler, *Phys. Rev. B* **51**, 1714 (1995); Y. Alhassid and C. H. Lewenkopf, *Phys. Rev. Lett.* **75**, 3922 (1995).  
 [6] A. M. Chang et al., *Phys. Rev. Lett.* **76**, 1695 (1996); J. A. Folk et al., *Phys. Rev. Lett.* **76**, 1699 (1996).  
 [7] S. W. McDonald, Lawrence Berkeley Lab. Report LBL-14837 (1983).  
 [8] E. J. Heller, *Phys. Rev. Lett.* **53**, 1515 (1984); E. B. Bogomolny, *Physica D* **31**, 169 (1988); M. V. Berry, *Proc. Roy. Soc. A* **243**, 219 (1989).  
 [9] L. Kaplan and E. J. Heller, *Ann. Phys. (N. Y.)* **264**, 171 (1998); a recent review appears in L. Kaplan, *Nonlinearity* **12**, R1 (1999).  
 [10] L. Kaplan, *Phys. Rev. E* **59**, 5325 (1999).  
 [11] L. Kaplan, *Phys. Rev. Lett.* **80**, 2582 (1998).  
 [12] S. Tomsovic and E. J. Heller, *Phys. Rev. Lett.* **67**, 664 (1991); *Phys. Rev. E* **47**, 282 (1993); L. Kaplan, *Phys. Rev. E* **58**, 2983 (1998).  
 [13] U. Sivan et al., *Phys. Rev. Lett.* **77**, 1123 (1996); S. R. Patel et al., *Phys. Rev. Lett.* **80**, 4522 (1998); Y. Alhassid, Ph. Jacquod, and A. Wobst, cond-mat/9909066.  
 [14] Y. Alhassid and C. H. Lewenkopf, *Phys. Rev. B* **55**, 7759 (1997).  
 [15] L. Kaplan and E. J. Heller, *Phys. Rev. E* **59**, 6609 (1999).  
 [16] A. Bäcker, R. Schubert and P. Stifter, *J. Phys. A* **30**, 6783 (1997); G. Tanner, *J. Phys. B* **30**, 2863 (1997); P.W. O'Connor and E.J. Heller, *Phys. Rev. Lett.* **61**, 2288 (1989).  
 [17] Y. Alhassid, M. Gökcedag, and A. D. Stone, *Phys. Rev. B* **58**, R7524 (1998).